Mode suppression in the non-Markovian limit by time-gated stimulated photon echo

de Boeij, W.P.; Pshenitchnikov, Maxim; Wiersma, D. A.

Published in:
Journal of Chemical Physics

DOI:
10.1063/1.472812

Publication date:
1996

Mode suppression in the non-Markovian limit by time-gated stimulated photon echo

Wim P. de Boeij, Maxim S. Pshenichnikov, and Douwe A. Wiersma
Ultrafast Laser and Spectroscopy Laboratory, Department of Chemistry, Materials Science Centre, University of Groningen, Nijenborgh 4, 9747 AG Groningen, The Netherlands

(Received 4 December 1995; accepted 15 May 1996)

It is demonstrated that enhanced mode suppression in stimulated photon echo experiments can be obtained by *diagonal* time gating of the echo. This technique is especially important when the optical dynamics of the system is non-Markovian. A two-mode Brownian oscillator model is used to analyze the effect of time gating on the stimulated photon echo. The method is demonstrated on a dye solution of DTTCI in ethylene glycol at room temperature. Experimentally, time gating of the echo is accomplished by means of femtosecond phase-locked heterodyne detected stimulated photon echo. The vibrational dynamics in this system are explored by conventional stimulated photon echo experiments. Especially stimulated photon echo-maximum shift measurements are found to be particularly useful. © *1996 American Institute of Physics.* [S0021-9606(96)01932-0]

I. INTRODUCTION

In the quest of a better grasp of solvation dynamics advances in femtosecond laser technology have been crucial. Nowadays, in many laboratories, sub-100 fs optical pulses, based on the modelocked Ti:sapphire laser,[1–4] are routinely available for time-gated fluorescence experiments[5–8] to map out the time-dependent Stokes shift. From these measurements a solvation correlation function can be constructed that, in linear response theory, is directly connected to a bath correlation function that fully determines the linear and nonlinear optical response functions.[9] However, the state-of-the-art time resolution, inherently limited by the uncertainty principle, is currently about 50 fs.[6–8] Furthermore, some problems exist with the fitting of the decays at early times.[7,8]

Another sensitive probe of solvation dynamics is femtosecond (stimulated) photon echo.[10–21] The decay of this echo is used to obtain a nonlinear response function from which a solvation correlation function can be constructed. Although photon echo is a more indirect probe of solvation dynamics than time-gated fluorescence, its time resolution is superior because it is only set by the optical pulse length. An additional advantage of photon echo is that it is a multiple pulse experiment, which provides the opportunity to perform two-dimensional measurements of the echo response function. Recently, we[20] and others[21] showed that with a cavity-dumped fs Ti:sapphire laser[22] the photon echo can be time gated, providing yet another dimension for study of the echo dynamics.

Numerous studies have been devoted to systems comprised of a dye molecule dissolved in some solvent. The electronic transition in all of these dyes is dressed with intramolecular vibrations. Generally the high-frequency vibrations are expressed in the spectrum as sidebands, while the low-frequency vibrations are hidden in the spectrum. Ultrafast excitation of such a transition thus prepares a state (wave packet) that is a superposition of all vibronic states covered by the spectral bandwidth of the excitation pulse. Clear signatures of vibrational dynamics have been observed as quantum beats in the decay of the stimulated photon echo and in fs pump–probe experiments.[23,24] With sufficient time resolution quantum beats are also expected in time-resolved Stokes shift measurements as a result of intramolecular vibrational dynamics. Therefore, in order to capture the genuine solute–solvent dynamics, wave packet dynamics has to be accounted for in the analysis of the data, or by some means the quantum beat effect has to be suppressed.

Mims[25] was the first to consider the problem of mode suppression in the context of stimulated electron spin echo experiments, where the ground and excited state are often split by a hyperfine interaction. He showed that when in such an experiment the third excitation pulse is delayed with respect to the first one by the inverse frequency of the hyperfine splitting, the effect of the electron–nucleus interaction on the spin echo decay is cancelled. The system behaves in this case as if it were a two-level system. Shank and coworkers recognized the importance of mode suppression toward optical dephasing measurements. Building on Mims' ideas, they demonstrated this principle of mode cancellation in stimulated photon echo experiments on nanocrystals of CdSe[26,27] and on an oxazine dye[27,28] in solution. We will show, however, that mode suppression by *time-integrated* stimulated photon echo works only in systems that exhibit Bloch-type dynamics.

In this paper we demonstrate that enhanced mode suppression can be obtained by gating the stimulated photon echo (SPE) at the conventional echo time and in phase with the wave packet dynamics. This technique is particular relevant to systems whose dynamics cannot be described by the Bloch equations. A case in point is optical dynamics in solution. Recent fs photon echo experiments on dye solutions provide convincing evidence for the fact that the Bloch picture fails to describe optical dephasing in solution.[11–21] A more advanced model is needed to account for the fact that in solution there is no clear separation of time scales between the decay of optical coherence and the time scale of solute–solvent fluctuations. This novel technique for mode suppres-

sion is demonstrated on a dye solution of DTTCI (3,3′-diethylthiatricarbocyanine iodide) in ethylene glycol.

II. THEORETICAL BACKGROUND

The principle of mode suppression in stimulated photon echo[26–28] can be quickly grasped by inspection of the following expression for the echo decay in the presence of a single harmonic vibrational mode at frequency ω:

$$S(t_{12},t_{13}) \sim \exp\left(-4\frac{\Delta^2}{\omega^2}(1-\cos\,\omega t_{12}) \times (1-\cos\,\omega t_{13})\right)\exp\left(-4\frac{t_{12}}{T_2}\right). \tag{1}$$

Here $S(t_{12},t_{13})$ is the *time-integrated* photon echo intensity, t_{12} is the time between the first and the second and t_{13} the delay between the first and the third excitation pulses, Δ is the normalized electron–phonon coupling parameter, and T_2 is the optical dephasing time constant.

Equation (1), derived for a δ-pulse-excited Franck–Condon vibrational manifold and assuming the electronic transition to be overwhelmingly inhomogeneously broadened, shows that the echo intensity can be written as a product of two exponential functions: one due to wave packet motion, the other due to optical dephasing. From Eq. (1) it can directly be inferred that for $t_{13}=2\pi/\omega$ the effect of wave packet dynamics is nullified, while for $t_{13}=\pi/\omega$ the quantum beat modulation of the echo intensity is at maximum. For $t_{13}=t_{12}$, Eq. (1) describes the decay of the two-pulse photon echo, which in this case is strongly affected by wave packet dynamics. Although the physics of mode suppression is fully contained in Eq. (1), its use is limited to systems whose optical dynamics can be captured by the optical Bloch equations.

The appeal of the multimode Brownian oscillator (MBO) model towards a description of optical dynamics is its flexibility to cover a wide range of different situations, thereby surpassing the optical Bloch model. The MBO model is also attractive because it connects directly optical to solvation dynamics. The model has been described extensively in the literature,[9] so we will just mention a few points relevant to this paper. In the MBO model all intramolecular, intermolecular, and solvent motions are represented by harmonic oscillators that can be over- or underdamped. While a molecular vibration in this model is represented by an underdamped oscillator, solvent motion is simulated by a set of different overdamped Brownian oscillators.[29] In any case, a major role is played by the so-called line broadening function $g(t)$. Once $g(t)$ is known, all nonlinear optical response functions can be calculated, including the one that determines the response of the SPE. It has been shown that $g(t)$ is connected to the correlation function $M(t)$ in the following way:

$$g(t)=i\lambda\int_0^t d\tau M(\tau)+\Delta^2\int_0^t d\tau_1\int_0^{\tau_1} d\tau_2\; M(\tau_2). \tag{2}$$

In Eq. (2), λ is equal to half the distance between the first momenta of the absorption and emission spectra, and Δ is connected to the frequency ω and displacement d of the Brownian oscillator by the relation $\Delta^2=\omega^2 d^2[n(\omega)+\frac{1}{2}]$, with $n(\omega)$ the thermal occupation number. In the high temperature limit these two parameters, Δ and λ, are related by $\Delta^2\approx 2\lambda kT/\hbar$. The extension to a multimode model is straightforward; $g(t)$ is just the sum over single oscillator line broadening functions, $g_i(t)$: $g(t)=\Sigma\; g_i(t)$.

It can be shown that the stimulated photon echo intensity excitation can be expressed in terms of $g(t)$ as follows:[9]

$$\begin{aligned} I_{\mathrm{SPE}}(t,t_{13},t_{12}) = 4\cos^2[\mathrm{Im}\{&g(t)+g(t_{13}-t_{12}) \\ &-g(t+t_{13}-t_{12})\}]\exp[-2\,\mathrm{Re}\{g(t) \\ &+g(t_{12})-g(t_{13}-t_{12})+g(t+t_{13}-t_{12}) \\ &+g(t_{13})-g(t+t_{13})\}]. \end{aligned} \tag{3}$$

In Eq. (3) t is the time of the echo with respect to the third pulse. Note that in conventional SPE experiments the signal is measured using a slow detector, thereby integrating the intensity [Eq. (3)] over time t:

$$S(t_{13},t_{12})=\int_0^\infty I_{\mathrm{SPE}}(t,t_{13},t_{12})dt. \tag{4}$$

In this paper we discuss the simplest, yet nontrivial, system that exhibits non-Markovian dynamics, composed of an electronic transition coupled to a strongly overdamped solvent mode and to an undamped vibrational oscillator. For such a system the correlation function is

$$M(t)=\frac{\Delta_1^2\,\exp(-\Lambda t)+\Delta_2^2\,\cos(\omega t)}{\Delta_1^2+\Delta_2^2}, \tag{5}$$

where Λ is the inverse correlation time of the bath, Δ_1 and Δ_2 are the individual coupling strengths and ω is the frequency of the undamped (vibrational) oscillator. When this correlation function is introduced into Eq. (2), the total line broadening function $g(t)$ is found to be

$$g(t)=i\left(\frac{\lambda_1}{\Lambda}\right)[1-\exp(-\Lambda t)]+\frac{\Delta_1^2}{\Lambda^2}[\exp(-\Lambda t)+\Lambda t-1] + i\,\frac{\lambda_2}{\omega}\sin\,\omega t+\frac{\Delta_2^2}{\omega^2}(1-\cos\,\omega t). \tag{6}$$

Let us for the moment ignore the cosine modulation of the echo intensity in Eq. (3), and focus on the damping of the echo intensity. After substitution of Eq. (6), we observe, as in Eq. (1), that the echo decay function can be expressed as a product of two terms: one due to wave packet dynamics, the other due to optical dephasing.

From Eqs. (3) and (6) the vibrational contribution to the echo decay rate Γ, at the return time of the wave packet ($t_{13}=2\pi/\omega$), is found to be

$$\Gamma^{\mathrm{vib}}_{t_{13}=2\pi/\omega}(t)=\exp-\left(2\frac{\Delta_2^2}{\omega^2}\{1-\cos\,\omega(t-t_{12})\}\right). \tag{7}$$

In the Bloch case, where the echo emerges at a delay time identical to the separation between the first two pulses ($t=t_{12}$), the vibrational effect on the decay of the time-integrated stimulated echo vanishes, as demonstrated before.[25–28] In the non-Markovian limit, however, where the echo does not emerge at the time $t=t_{12}$,[20,21] mode cancellation cannot be achieved by detection of the time-integrated signal, simply because $t\neq t_{12}$ and hence the vibrational contribution given by Eq. (7) remains. Inspection of Eq. (7), however, shows that mode suppression can be recovered by *time gating* the stimulated photon echo polarization or intensity at time $t=t_{12}$. In this manner one probes only the echo polarization (or intensity) inside the time window provided by the gate pulse centered at the classical echo time $t=t_{12}$. We will refer to this echo detection method as diagonal time gating.

When the probe pulse is out of phase with the wave packet ($t_{13}=\pi/\omega$), we get for the vibrational damping constant

$$\Gamma^{\mathrm{vib}}_{t_{13}=\pi/\omega}(t)=\exp-\left(2\frac{\Delta_2^2}{\omega^2}\{3-2\cos\,\omega t-2\cos\,\omega t_{12}+\cos\,\omega(t-t_{12})\}\right). \tag{8}$$

Equation (8) shows that for diagonal time gating of the echo at the outer turning point of the wave packet a vibrational contribution remains that is identical to that of the Bloch limit [Eq. (1)].

Finally we wish to consider the effect of the cosine modulation on the echo intensity in the limit of optimal mode suppression. It is easily shown that under optimal conditions of mode suppression, $t=t_{12}$ and $t_{13}=2\pi/\omega$ and in the limit $\Lambda t_{13}\gg 1$, Eq. (3) becomes

$$I_{\mathrm{SPE}}(t)=4\cos^2\{(\lambda/\Lambda)[1-\exp(-\Lambda t)]\}\times\exp\left(-\frac{4\Delta_1^2}{\Lambda^2}[\exp(-\Lambda t)+\Lambda t-1]\right). \tag{9}$$

Equation (9), obtained under the conditions for optimal mode suppression, only contains terms due to the strongly overdamped solvent mode. Complete suppression of a vibrational wave packet contribution thus is possible. Note that for delays t, longer than the correlation time Λ^{-1} ($\Lambda t\gg 1$), the cosine part completely vanishes, and the exponential function in Eq. (9) reduces to a single exponential decay, with characteristic time $\tau_0=\Lambda/(4\Delta^2)$. From Eq. (9) it can also be deduced that for delays t shorter than the correlation time, the initial decay of the diagonal time-gated echo intensity is Gaussian.

Finally, let us reflect on how the Brownian oscillator model connects to the Bloch model. In the Bloch model, where the system dynamics can be separated into inhomogeneous (static) and homogeneous (fast) dynamical processes,[9] the line broadening function of the solvent mode can be expressed as $g(t)=t/T_2+\Delta^2t^2/2$. The first term describes the homogeneous dephasing part, while the second one represents the inhomogeneous broadening. Under these conditions and in the limit of overwhelming inhomogeneous broadening $\Delta\gg 1/T_2$, Eqs. (3) and (4) reduce to Eq. (1) with $t=t_{12}$ (Bloch–Hahn echo).

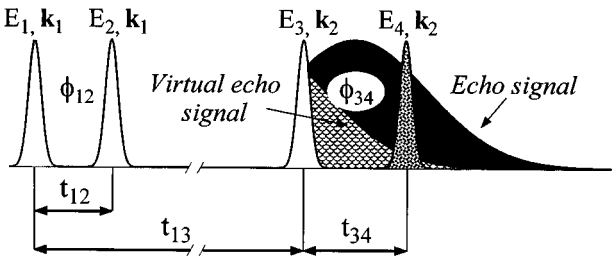

FIG. 1. Pulse sequence for phase-locked heterodyne detected stimulated photon echo; ϕ_{12} and ϕ_{34} denote the relative phases between pulses E_1-E_2 and E_3-E_4, respectively, while $\mathbf{k}_1$ and $\mathbf{k}_2$ stand for their wave vectors.

Summarizing the results of this section: By diagonal time gating of the SPE in phase with the wave packet recurrence time, the vibrational contribution to the echo decay can be fully suppressed. This result is more general than for the model chosen comprised of two Brownian oscillators. As in the MBO model all oscillators are independent; by diagonal time gating of the SPE we can nullify the effect of *any* oscillator whose dynamics is slower than the first-third pulse delay time. This is an important virtue of the time-gated SPE as in most cases the optical dynamics cannot be captured by use of just two Brownian oscillators.

In closing this section we compare the time-gated SPE with fifth-order three-pulse scattering spectroscopy[30,31] (FOTS), introduced by Cho and Fleming as a tool to separate homogeneous and inhomogeneous broadening. Briefly, in FOTS the optical polarization excited by two pulses is interrogated in the sample by a third pulse. Thus FOTS can be considered as a form of time-gated two-pulse photon echo spectroscopy, be it that its theoretical description and numerical calculation are more involved. While diagonal FOTS in certain limits can aid in the suppression of slow solvent motions (inhomogeneous broadening at the time scale of the experiment), it cannot be used for the cancellation of underdamped modes. Thus the decay of diagonal FOTS is still strongly affected by wave packet dynamics.

III. EXPERIMENT

The experimental realization of the time-gated stimulated photon echo was accomplished by performing phase-locked heterodyne-detected stimulated photon echo (PL-HSPE) experiments.[32–34] The concept of PL-HSPE was introduced by Cho *et al.*[32] while the first experiment of this kind was realized by de Boeij *et al.*[34] The pulse sequence for PL-HSPE is shown in Fig. 1. Briefly, three ultrashort pulses E_1, E_2, and E_3 induce a third-order polarization $P^{(3)}(t)$ on the optical transition. The resulting time-dependent signal field $E(t)\sim P^{(3)}(t)$ is interfered with a fourth replica pulse E_4. The fourth pulse E_4 acts both as a local oscillator for the heterodyne detection and as the desired femtosecond gate pulse of the photon echo signal. Since the signal field has a much smaller amplitude than that of the fourth pulse:

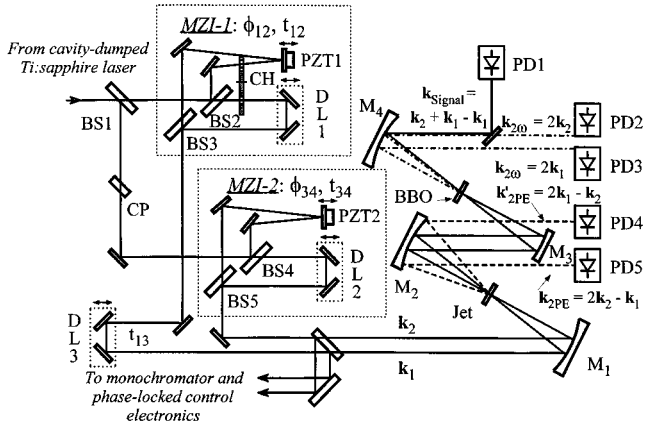

FIG. 2. Experimental setup for phase-locked heterodyne detected stimulated photon echo experiments. MZI—Mach–Zehnder interferometer; BS—$T=50\%$ femtosecond beamsplitters; PZT—piezoelectrical transducer; DL—delay line; CH—double-slot mechanical chopper; CP—compensation plate; M—$r=25$ cm focusing mirrors; Jet—100-μm thick jet containing a sample; BBO—100-μm thick β-barium borate crystal; PD—photodiodes.

$|E(t)| \ll |E_4|$, the heterodyne detected signal becomes $S(t_{34}) \propto \mathrm{Re}[E(t)E_4^*(t_{34})]$. Note that in phase-locked photon echo it is essential that in each pulse pair the pulses are collinear[32,34] to have the optical phase defined properly across the beam.

The alternative method, conventional time-gated photon echo,[20,21] was also explored but yielded signals with inferior signal-to-noise ratio. In the echo upconversion case, the signal is proportional to $S \propto |E(t)|^2 \kappa |E_g|^2$, where κ is some constant depending on several factors (nonlinear susceptibility of the crystal, frequencies of the fields, etc.) and $|E_g|^2$, the gating pulse intensity. Because of the nature of the upconversion process from fundamental to second harmonic, the upconversion efficiency is always $\kappa |E_g|^2 \leqslant 2$. Therefore, the heterodyne-detected signal exceeds by far the time-gating signal. In addition to enhanced sensitivity, the heterodyne-detected signal preserves the phase of the echo polarization. By controlling the phase difference (0 or $\pi/2$) between the third and fourth excitation pulses, the real and imaginary part of the third-order polarization created in the sample can thus be probed.

The phase-locked photon echo experiments were performed with a setup displayed in Fig. 2. The heart of the setup is formed by a home-built, 13-fs cavity-dumped Ti:sapphire laser operated at a repetition rate of 4 MHz.[22] The laser output was sent into a prism compressor to precompensate for dispersion in the optical elements of the setup, then split into two beams (BS1) which were directed into two identical Mach–Zehnder interferometers. Each interferometer produced a pair of interferometrically stable pulses E_1 and E_2 (MZI-1) and E_3 and E_4 (MZI-2). The delays t_{12} and t_{34} and relative phases ϕ_{12} and ϕ_{34} between pulses in each pair were precisely controlled by translation stages (DL1 and DL2) and piezo transducers (PZT1 and PZT2). Both phases could be set independently at 0 or $\pi/2$ (or any other value) and were kept constant at any delay t_{12}, t_{34} using tracking feedback loops.[35,36] Furthermore, active stabilization of the interferometers prevented phase drifts caused by low-frequency acoustic or thermal perturbations.

After the interferometers the two pulse pairs were delayed by a time t_{13} (DL3) and focused into a sample jet using all reflective optics to minimize the overall dispersion. Dye solutions of DTTCI (Lamda Physik) in ethylene glycol (EG) were made with a peak optical density of less than 0.2 over a jet thickness of 100 μm. The energies of all pulses were about equal and did not exceed 170 pJ per pulse ($\sim$0.7 mW of average power) at the sample. Such low intensities were necessary to exclude high-order ($\chi^{(5)}$, etc.) nonlinear optical effects. The absence of effects due to accumulation of pulse-pair excitations was assured by also performing experiments with lower repetition rates. Great care was taken to equalize the dispersion along each beam pathway to avoid uncompensated frequency chirp.

The PL-HSPE signals were detected by a silicon photodiode (PD1) placed in the beam that carries the pulses E_3 and E_4, and processed by a lock-in amplifier. The amplifier was referenced to the sum frequency of the double-slot chopper (CH) that modulated beams E_1 and E_2. The collinear cross correlation of pulses E_3 and E_4 gives, at any delay time, a pure dc signal which is not detected by the lock-in amplifier. Three distinct contributions to the signal remain due to the possible permutations of the pulses: E_1-E_2-E_3-E_4, E_1-E_2-E_3-E_3, and E_1-E_2-E_4-E_4. The first pulse sequence yields the true PL-HSPE signal while the latter two combinations lead to phase-locked pump–probe signals.[32] In the heterodyne detection scheme employed, all three signals just add at the detector, without any cross interference. To obtain the phase-locked photon echo signal we first performed a measurement with all four beams (Fig. 1). Subsequently experiments were done with pulse E_3 blocked, followed by a measurement where pulse E_4 was impeded. One gets the genuine PL-HSPE signal by subtracting the sum of the latter two phase-locked pump–probe signals from the signal detected with all four beams.

Along with PL-HSPE we also registered several other signals to determine the zero-delay points between pulses. These signals were also used as a reference in feed-back loops for stabilizing the setup at long times. Interferometric second harmonic autocorrelations of pulse pairs E_1-E_2 and E_3-E_4 were detected by photodiodes PD2 and PD3 after refocusing the excitation beams into a thin BBO crystal. Two-pulse photon echoes into conjugated directions $\mathbf{k}_{2PE}=2\mathbf{k}_2-\mathbf{k}_1$ and $\mathbf{k}'_{2PE}=2\mathbf{k}_1-\mathbf{k}_2$ were picked off by photodiodes PD4 and PD5 to determine the delay t_{13} between the first and the third pulses. During the experiments, all auxiliary signals were surveyed regularly and possible drifts in zero delay points registered and accounted for.

Time-integrated SPE experiments were performed with a different setup and using a conventional box geometry as described in Ref. 37. Briefly, three beams with wave vectors $\mathbf{k}_1$, $\mathbf{k}_2$, and $\mathbf{k}_3$ were crossed under a small angle in the sample (Fig. 3, inset). The stimulated photon echo signals were simultaneously detected at $\mathbf{k}_3+\mathbf{k}_2-\mathbf{k}_1$ and $\mathbf{k}_3-\mathbf{k}_2+\mathbf{k}_1$ directions by silicon photodiodes.

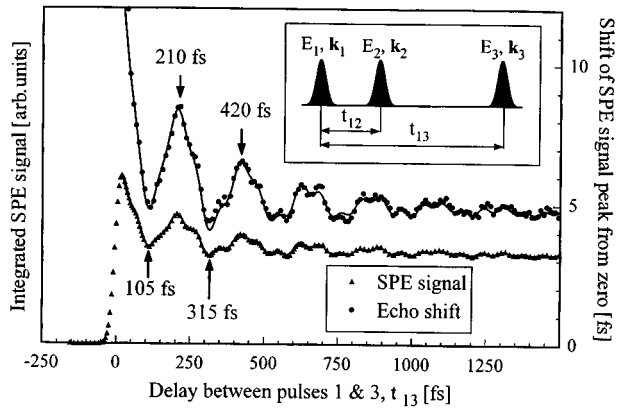

FIG. 3. Integrated stimulated photon echo signal (▲), the echo-shift from zero (●), and fits as described in the text (solid lines). Parameters of fits are given in Table I. The inset shows a pulse sequence in the experiment. The delay between the first and the second excitation pulse for the integrated stimulated photon echo signal is set on $t_{12}=20$ fs.

IV. RESULTS AND DISCUSSION

A. Optically active vibrational modes probed by conventional stimulated photon echo

To perform mode suppression experiments we need first to characterize the active vibrational modes. A well-known probe for vibrational activity is the conventional stimulated photon echo (SPE).[11,16,26–28] Figure 3 displays the time-integrated SPE signal as a function of the waiting time t_{13}. The observed quantum beats in the SPE signal are caused by the coupling of the optical transition to several vibrational modes. A fit to the SPE signal with the function $\Sigma_i A_i \exp(-\Lambda_i t)\cos(\omega_i t)$ yields three vibrational modes with frequencies of 153, 377, and 485 cm^{-1} (Table I). Although the frequencies of these modes are determined quite accurately, their amplitudes are not. Why this is so can readily be understood by inspection of Eq. (1). This equation shows that when t_{13} is scanned, no oscillations occur for $\omega t_{12}=0$, 2π, 4π, etc., while for $\omega t_{12}=\pi$, 3π, etc., the amplitude of this oscillation is at maximum. The relative amplitudes of the different vibrational modes in the SPE decay thus varies with t_{12}. For instance, if t_{12} is set at 60 fs, the 485 cm^{-1} mode virtually disappears in the stimulated photon echo decay.

TABLE I. Parameters obtained from the fits displayed in Fig. 3. The amplitudes are normalized so their sum is unity. To allow comparison with Fig. 3 all amplitudes for the peak shift should be multiplied by 14 fs.

	A_i		Λ_i (ps^{-1})		ω_i (cm^{-1})	
	SPE	Peak shift	SPE	Peak shift	SPE	Peak shift
1	0.17	0.24	2.9	2.6	153	153
2	0.02	0.02	0.9	1.0	485	480
3	0.01	0.007	1.2	1.15	377	380
4	0.28	0.35	6.6	7.2	0	0
5	0.14	0.12	0.21	0.15	0	0
6	0.38	0.25	0	0	0	0

More quantitative information on the vibrational mode amplitudes (including the low-frequency ones) can be obtained from a measurement of the so-called echo-maximum shift function.[14,37] In this experiment the shift of the time-integrated SPE echo maximum with respect to $t_{12}=0$ is measured when the delay time t_{12} is scanned, for a particular waiting time t_{13}. A plot of this shift versus the waiting time t_{13} presents the echo shift function. *We found in computer simulations[38] and later showed analytically[39] that the echo shift function reflects surprisingly well the correlation function $M(t_{13})$* and consequently is an excellent probe of the relative amplitudes for the different active vibrational modes. To determine the echo-peak shift, stimulated photon echo signals in conjugated directions: (i) $\mathbf{k}_3+\mathbf{k}_2-\mathbf{k}_1$ and (ii) $\mathbf{k}_3+\mathbf{k}_1-\mathbf{k}_2$ were measured simultaneously. For (i) the delay t_{12} is scanned only, while for (ii) both t_{12} and t_{13} are scanned synchronously to keep the delay between the first and the last excitation pulse (as they arrive at the sample) fixed. The measured echo profiles were fit to Gaussians while the shift was calculated as half the distance between the two echo maxima. In this manner effects due to long-term thermal drift of the experimental setup are accounted for. The results of these measurements are displayed in Fig. 3 as solid circles, along with a fit based on a damped cosines function. The corresponding parameters are given in Table I. From the scatter in the data at long delays the accuracy of the echo-maximum shift measurements is estimated to be $\sim\frac{1}{4}$ fs.

Next to the frequencies of the underdamped vibrational modes, Table I contains also the damping constants of the underdamped vibrational modes and overdamped solvent modes. Note that for the overdamped solvent modes the fit function $\Sigma_i A_i \exp(-\Lambda_i t)\cos(\omega_i t)$ reduces to $\Sigma_i A_i \exp(-\Lambda_i t)$. This is expressed in Table I by putting $\omega_i=0$. While the vibrational modes decay on a picosecond time scale, the fastest solvent mode decays in about 140 fs. Solvation dynamics occurs also on a time scale of 7 ps and on much longer time scales, included here as a base line. These slow dynamical processes lead to inhomogeneous broadening of the optical transition on a time scale of less than 1 ps. Recently performed phase-locked pump–probe measurements[40] show that the fastest solvation event in DTTCI in ethylene glycol occurs in about 50 fs. This initial ultrafast process does not manifest itself in echo shift measurements, probably because it occurs in the time window where the excitation pulses overlap in time.

The occurrence of quantum beats in the echo-maximum shift has recently been reported[34] and can be explained as follows. It is well known[37] that the echo-maximum shift is a measure of the relative weight of homogeneous versus inhomogeneous broadening. For small delays $(t,t_{12} \ll 2\pi/\omega)$, the term that describes wave packet motion in Eq. (3) becomes $\exp[-\Delta^2(t^2+t_{12}^2-2tt_{12}\cos\omega t_{13})]$. For $t_{13}=2\pi/\omega$ this expression reduces to $\exp[-\Delta^2(t-t_{12})^2]$. A vibrational mode (manifold) thus generates a certain ''inhomogeneous'' broadening at $t_{13}=2\pi/\omega$. Thus for small delays a vibration-dressed optical transition can produce an echo signal, even in case it is entirely *homogeneously* broadened.[41] Figure 3 demonstrates that when the wave

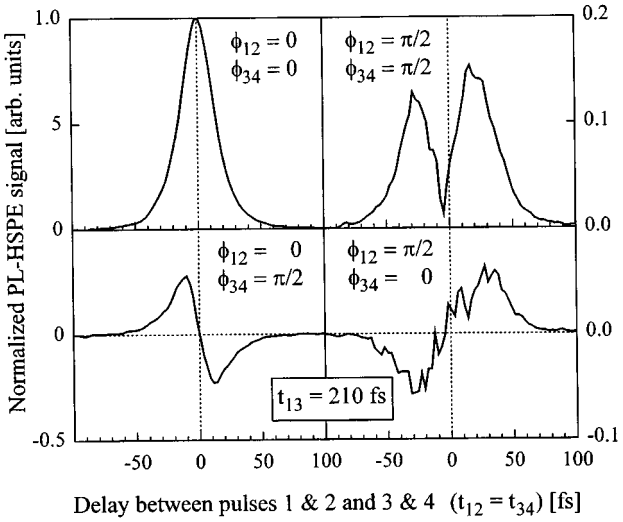

FIG. 4. Diagonal phase-locked heterodyne detected stimulated photon echo signals for different combinations of phases ϕ_{12} and ϕ_{34} taken at the delay time between the first and the third excitation pulses $t_{13}=210$ fs. Note that the intensity scale for the $\phi_{12}=\pi/2$ signals is magnified by factor of 5.

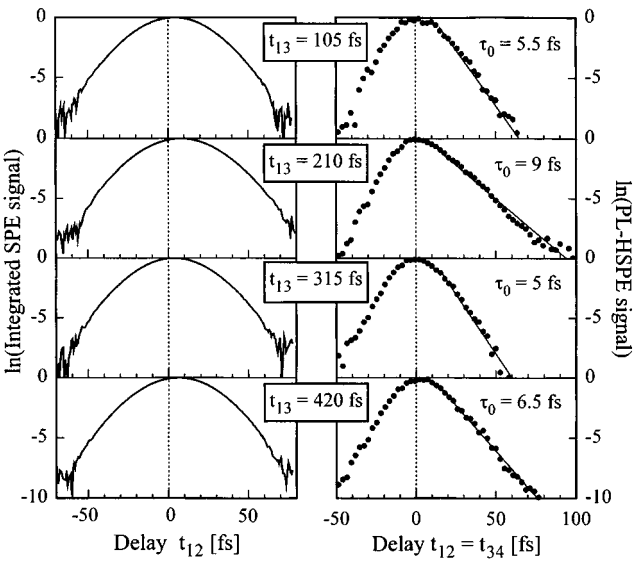

FIG. 5. Mode suppression in time-integrated (left panel) versus time-gated (right panel) stimulated photon echo experiments. Diagonal time-gated signals are obtained as described in the text. Conventional and virtual echoes are shown for positive and negative delay times, respectively. The solid lines in the right panel are fits to the time-gated echo signals with the function $-t_{12}/\tau_0$.

packet recurs at $t_{13}=2\pi/\omega,4\pi/\omega$, etc., the ''vibrational inhomogeneity'' reaches a maximum, as reflected in the echo shift.

Table I shows that the lowest frequency mode is the most prominent one and hence the prime candidate for mode suppression. However, the effect of the other two modes on optical dephasing can also effectively be cancelled. Of course, there is some luck involved here. One fortunate incident is the fact that the 485 cm^{-1} mode has a frequency of about three times that of the 153 cm^{-1} mode. This means that at the first recurrence of the low-frequency mode, the 485 cm^{-1} mode is close to its third return. As far as the third mode is concerned, its relative amplitude is negligible at early times ($t_{13}<300$ fs). For practical purposes we can thus state that the wave packet refocusses at $t_{13}\sim 210$ fs and $t_{13}\sim 420$ fs, while at $t_{13}\sim 105$ fs and $t_{13}\sim 315$ fs it is at its most remote position.

B. Mode suppression in time-resolved stimulated photon echo

Now that we have mapped out the wave packet dynamics we can attempt to suppress its effect on the echo decay by time gating of the echo at the appropriate delay time. Figure 4 displays a series of diagonal time-gated ($t_{12}=t_{34}$) PL-HSPE signals $S(\phi_{12},\phi_{34})$ probed at $t_{13}=210$ fs for different combinations of the phases ϕ_{12} and ϕ_{34}. Similar experiments were done at the other characteristic waiting times indicated by arrows in Fig. 3. The observed mirror or inversion symmetry of the traces is due to the fact that pulses E_1 and E_2, and E_3 and E_4, are indistinguishable and thus may change roles when the delays t_{12} and t_{34} are scanned.

It has been shown[34] that four different Liouville pathways contribute to the measured PL-HSPE signal. Of these four, only the two so-called rephasing pathways contribute to the conventional SPE signal. The other two nonrephasing transition amplitudes generate a polarization that leads to the so-called virtual echo.[42,43] Mathematically, the virtual echo has the same temporal profile as the real echo but it peaks *before* the third excitation pulse. Causality demands that only its tail can be observed experimentally, as depicted in Fig. 1. The possibility of selecting the phase differences in the pulse sequence, combined with the fact that the heterodyne-detected signal is the sum of the polarizations induced via the different Liouville pathways,[9,34] allows us to disentangle the various contributions to the signal. The four signals, recorded with indicated phase settings ϕ_{12} and ϕ_{34} (Fig. 4), form an orthogonal base. From these phase-locked echo signals the conventional photon echo intensity expressed in Eq. (3) can be obtained by performing the following operation:[32,44]

$$I_{\mathrm{SPE}}=\left[S(\phi_{12}=0;\ \phi_{34}=0)+S\left(\phi_{12}=\frac{\pi}{2};\ \phi_{34}=\frac{\pi}{2}\right)\right]^2 + \left[S\left(\phi_{12}=\frac{\pi}{2};\ \phi_{34}=0\right)-S\left(\phi_{12}=0;\ \phi_{34}=\frac{\pi}{2}\right)\right]^2. \tag{10}$$

Although the conventional echo by itself is sufficient to demonstrate enhanced mode suppression, we address the virtual echo as well since it shows a distinctly different behavior compared to the usual echo signal. The virtual echo signal is obtained from Eq. (10), when the plus and minus signs inside the square brackets are interchanged.

Figure 5 compares the results obtained for time-integrated versus diagonal time-gated photon echo experiments. In the conventional time-integrated technique (the left panel) the echo decays are virtually independent of whether

the third pulse is in or out of phase with the rephasing wave packet. Moreover, even the shape of the echo traces is nearly the same for all waiting times. The only difference, but barely noticeable, is in the position of the maximum, which is slightly shifted from zero (5 fs at 105 fs vs 8.5 fs at 210 fs, Fig. 3) depending on the time t_{13}.

In striking contrast, in the time-gated case the echo decays are found to be strongly dependent on the timing of the third pulse (Fig. 5, the right panel). Here, for $t_{12}>0$ we display the echo signal for which mode suppression is expected [Eq. (7)]. The virtual echo signal is displayed for $t_{12}<0$. Note that with heterodyne detection of the echo a dynamical range of about five decades is obtained. From the results presented it is quite clear that diagonal time gating of the stimulated echo leads to enhanced mode suppression for systems that exhibit non-Markovian optical dynamics, in accordance with the analysis in Sec. II. For $t_{13}=210$ fs, where maximal mode suppression is expected, the echo signal can be measured up to $t_{12}=100$ fs. The slope of the signal is found to be almost linear, which corresponds to an exponentially decaying echo signal with a time constant of about 9 fs. In the Markovian limit such a decay time corresponds to an optical dephasing time T_2 of 36 fs. The fact that the integrated echo signal (the left panel) exhibits no signature of mode suppression proves, however, that the system dynamics is non-Markovian.[34] Of course, this had been established before, most notably by the finding of an imaginary component in $g(t)$,[40] which cannot occur in the Bloch model. The observed exponential decay of the time-gated echo for $t_{13}=210$ fs thus necessitates the presence of an ultrafast non-Markovian process, whose correlation time is $\sim$20 fs [Eq. (9) and discussion following]. This conclusion accords with recent phase-locked pump–probe experiments which provide a correlation time of $\sim$50 fs for this system.[40]

For longer delays of the third pulse, the time-gated echo decays become increasingly faster. The reason for this behavior is threefold: First, solvent modes that could be considered inhomogeneous for short waiting times t_{13} (Table I) do affect the echo decay now. Time gating can no longer suppress the effect of these modes, which results in an enhanced decay. Second, so far we have considered an undamped vibrational mode [Eq. (5)]. Of course, in reality vibrational coherence has a finite decay time ($\sim$350 fs for the 153 cm^{-1} mode, Table I). This decay is irreversible and therefore cannot be eliminated by time gating. Third, the presence of different vibrational frequencies in the excited wave packet results in mode dispersion for longer waiting times t_{13}. As the amplitude of the more prominent vibrational mode (at 153 cm^{-1}) declines, the other two become more important in the dynamics. Taking into account the frequency differences, there is hardly a point where all three modes act in phase. On the contrary, at $t_{13}=655$ fs, the phase of the 153 cm^{-1} mode opposes almost precisely the phases of the other two modes (Fig. 3). Consequently no mode suppression is expected nor has been observed at this delay.

Unlike the echo signals, the diagonal-gated virtual echo signals ($t_{12}<0$) look very much the same at all waiting times t_{13} (Fig. 5). As was shown, by diagonal time gating, the inhomogeneous contribution (that is, slow on the experimental time scale) is efficiently removed from the conventional echo signal due to rephasing of nonlinear polarization. No such rephasing is possible for the virtual echo. Therefore, time gating at $t=t_{12}$ in this case leads to a fast decay that is mainly determined by the inverse width of the whole absorption spectrum,[43] convoluted with the experimental temporal resolution. On the other hand, this simple picture is complicated by the presence of the vibrational modes. Calculations similar to Sec. IV A show that when the wave packet is at its outer turning point ($t_{13}=\pi/\omega$, $3\pi/\omega$, etc.), the vibrational contribution to the virtual echo decay reduces to $\exp[-\Delta^2(t-t_{12})^2]$. The apparent vibrational rephasing, however, is strongly counteracted by (nonrephasing) slow dynamical processes. In fact, a very faint modulation of the virtual echo decay at different waiting times is expected due to a relatively small weight of the vibrational modes (about 25%, Table I). An indication of mode suppression for the virtual echo is that the decays at $t_{13}=105$ fs and $t_{13}=315$ fs are slightly longer than the one at $t_{13}=210$ fs (Fig. 5).

Compared to the conventional echo, the virtual echo signals always exhibit somewhat faster decays independently of the wave packet motion. This fact is a clear signature of appreciable inhomogeneous broadening at the time scale of the experiment. By diagonal time gating, the effect of inhomogeneous broadening is effectively cancelled in the conventional but not the virtual echo. Note that neither of the effects discussed above can be observed in the time-integrated echo case.

In summary, we have demonstrated that diagonal time gating of the stimulated photon echo leads to mode suppression in the non-Markovian limit. We have employed a heterodyne-detected stimulated photon echo technique to construct the time-resolved echo signals with enhanced signal to noise ratio. In a separate paper we will show that manipulation of phase-locked detected echo signals enables one to construct all possible four-wave mixing signals.[44] Results similar to the ones reported here have been obtained using a homodyne-detected time-gated echo scheme.[45] However, we found that the echo detected in this fashion is severely distorted by interference effects due to stray light, despite the fact that the optical phase of the gate pulse was scrambled.

Multiple pulse photon echo, of course, has much in common with multiple-pulse NMR. In NMR a great variety of pulse techniques have been developed which allow dissection of various interactions. Compared to the sophistication of multiple-pulse NMR,[46] multiple-pulse optical experiments have a long way to go. For instance, it remains a formidable challenge to suppress not only a single underdamped mode, but all modes at different frequencies. Future experiments are aimed at further development of nonlinear optical multiple pulse experiments with the ultimate goal to dissect the solute–solvent dynamics from intramolecular effects.

ACKNOWLEDGMENTS

We are grateful to F. de Haan for providing us with software for efficient data collection and handling. Special

thanks are due to R. Szipöcs and K. Ferencz for the design and manufacturing of femtosecond beamsplitters. The investigations were supported by the Netherlands Foundation for Chemical Research (SON) and Physical Research (FOM) with financial aid from the Netherlands Organization for the Advancement of Science (NWO).

[1] D. E. Spence, P. N. Kean, and W. Sibbett, Opt. Lett. **16**, 42 (1991).
[2] P. F. Curley, Ch. Spielmann, T. Brabec, F. Krausz, E. Winter, and A. J. Schmidt, Opt. Lett. **18**, 54 (1993).
[3] M. Asaki, C. Huang, D. Garvey, J. Zhou, H. C. Kapteyn, and M. M. Murnane, Opt. Lett. **18**, 977 (1993).
[4] A. Stingl, M. Lenzner, C. Spielmann, F. Krausz, and R. Szipöcs, Opt. Lett. **20**, 602 (1995).
[5] M. Cho, S. J. Rosenthal, N. F. Scherer, L. D. Ziegler, and G. R. Fleming, J. Chem. Phys. **96**, 5033 (1992).
[6] R. Jimenez, G. R. Fleming, P. V. Kumar, and M. Maroncelli, Nature **369**, 471 (1994); S. J. Rosenthal, R. Jimenez, G. R. Fleming, P. V. Kumar, and M. Maroncelli, J. Mol. Liq. **60**, 25 (1994).
[7] M. L. Horng, J. Gardecki, A. Papazyan, and M. Maroncelli, J. Phys. Chem. **99**, 17311 (1995).
[8] T. Gustavsson, G. Baldacchino, J.-C. Mialocq, and S. Pommeret, Chem. Phys. Lett. **236**, 587 (1995).
[9] S. Mukamel, *Principles of Nonlinear Optical Spectroscopy* (Oxford University Press, New York, 1995).
[10] P. C. Becker, H. L. Fragnito, J. Y. Bigot, C. H. Brito Cruz, R. L. Fork, and C. V. Shank, Phys. Rev. Lett. **63**, 505 (1989).
[11] J. Y. Bigot, M. T. Portella, R. W. Schoenlein, C. J. Bardeen, A. Migus, and C. V. Shank, Phys. Rev. Lett. **66**, 1138 (1991).
[12] E. T. J. Nibbering, D. A. Wiersma, and K. Duppen, Phys. Rev. Lett. **66**, 2464 (1991).
[13] E. T. J. Nibbering, K. Duppen, and D. A. Wiersma, J. Photochem. Photobiol. A: Chem. **62**, 347 (1992).
[14] T. Joo and A. C. Albrecht, Chem. Phys. **176**, 233 (1993).
[15] E. T. J. Nibbering, D. A. Wiersma, and K. Duppen, Chem. Phys. **183**, 167 (1994).
[16] K. Duppen, E. T. J. Nibbering, and D. A. Wiersma, in *Femtosecond Reaction Dynamics*, edited by D. A. Wiersma (North Holland, Amsterdam, 1994), p. 197.
[17] W. P. de Boeij, M. S. Pshenichnikov, K. Duppen, and D. A. Wiersma, Chem. Phys. Lett. **224**, 243 (1994).
[18] C. J. Bardeen and C. V. Shank, Chem. Phys. Lett. **226**, 310 (1994).
[19] P. Vöhringer, D. C. Arnett, R. A. Westervelt, M. J. Feldstein, and N. F. Scherer, J. Chem. Phys. **102**, 4027 (1995).
[20] M. S. Pshenichnikov, K. Duppen, and D. A. Wiersma, Phys. Rev. Lett. **74**, 674 (1995).
[21] P. Vöhringer, D. C. Arnett, T.-S. Yang, and N. F. Scherer, Chem. Phys. Lett. **237**, 387 (1995).
[22] M. S. Pshenichnikov, W. P. de Boeij, and D. A. Wiersma, Opt. Lett. **19**, 572 (1994).
[23] H. L. Fragnito, J.-Y. Bigot, P. C. Becker, and C. V. Shank, Chem. Phys. Lett. **160**, 101 (1989); W. T. Pollard, H. L. Fragnito, J.-Y. Bigot, C. V. Shank, and R. A. Mathies, Chem. Phys. Lett. **168**, 239 (1990).
[24] P. Cong, Y. J. Yan, H. Deuel, and J. D. Simon, Chem. Phys. Lett. **212**, 367 (1993); J. Chem. Phys. **100**, 7855 (1994).
[25] W. B. Mims, Phys. Rev. B **5**, 2409 (1972); Phys. Rev. B **6**, 3543 (1972).
[26] R. W. Schoenlein, D. M. Mittleman, J. J. Shiang, A. P. Alivisatos, and C. V. Shank, Phys. Rev. Lett. **70**, 1014 (1993).
[27] C. V. Shank, R. W. Schoenlein, C. J. Bardeen, and D. M. Mittleman, in *Femtosecond Reaction Dynamics*, edited by D. A. Wiersma (North Holland, Amsterdam, 1994), p. 125.
[28] C. J. Bardeen and C. V. Shank, Chem. Phys. Lett. **203**, 535 (1993); **226**, 310 (1994).
[29] L. E. Fried, N. Bernstein, and S. Mukamel, Phys. Rev. Lett. **68**, 1842 (1992).
[30] M. Cho and G. R. Fleming, J. Chem. Phys. **98**, 3478 (1994).
[31] T. Joo, Y. Jia, and G. R. Fleming, J. Phys. Chem. **102**, 4063 (1995).
[32] M. Cho, N. F. Scherer, G. R. Fleming, and S. Mukamel, J. Chem. Phys. **96**, 5618 (1992).
[33] M. Cho and G. R. Fleming, J. Chem. Phys. **98**, 2848 (1993).
[34] W. P. de Boeij, M. S. Pshenichnikov, and D. A. Wiersma, Chem. Phys. Lett. **238**, 1 (1995).
[35] N. F. Scherer, A. J. Ruggiero, M. Du, and G. R. Fleming, J. Chem. Phys. **93**, 856 (1990).
[36] N. F. Scherer, R. J. Carlson, A. Matro, M. Du, A. J. Ruggiero, V. Romero-Rochin, J. A. Cina, and G. R. Fleming, J. Chem. Phys. **95**, 1487 (1991).
[37] S. De Silvestri, A. M. Weiner, J. G. Fujimoto, and E. P. Ippen, Chem. Phys. Lett. **112**, 195 (1984); A. M. Weiner, S. De Silvestri, and E. P. Ippen, J. Opt. Soc. Am. B **2**, 654 (1985).
[38] D. A. Wiersma, W. P. de Boeij, and M. S. Pshenichnikov, ''Time-resolved femtosecond photon echo as probe of solvent motion,'' invited paper at the Time Resolved Vibrational Spectroscopy-7 Meeting, Santa Fé, New Mexico, June 1995.
[39] W. P. de Boeij, M. S. Pshenichnikov, and D. A. Wiersma, Chem. Phys. Lett. **253**, 53 (1996).
[40] W. P. de Boeij, M. S. Pshenichnikov, and D. A. Wiersma, Chem. Phys. Lett. **247**, 264 (1995).
[41] G. Stock, J. Chem. Phys. **101**, 246 (1994).
[42] R. L. Schoemaker, in *Laser and Coherence Spectroscopy*, edited by J. I. Steinfeld (Plenum, New York, 1978), p. 294.
[43] K. Duppen and D. A. Wiersma, J. Opt. Soc. Am. B **3**, 614 (1986).
[44] W. P. de Boeij, M. S. Pshenichnikov, and D. A. Wiersma (unpublished).
[45] M. S. Pshenichnikov, W. P. de Boeij, and D. A. Wiersma (unpublished).
[46] R. R. Ernst, G. Bodenhausen, and A. Wokaun, ''Principles of nuclear magnetic resonance in one and two dimensions,'' in *The International Series on Monographs on Chemistry* (Clarendon, Oxford, 1987), Vol. 14.